Accepted Manuscript

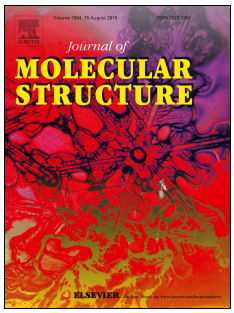

Synthesis, growth, structure and characterization of chalcone crystal: A novel organic NLO material

R. Agilandeshwari, V. Meenatchi, S.P. Meenakshisundaram

PII: S0022-2860(16)30193-4

DOI: 10.1016/j.molstruc.2016.02.099

Reference: MOLSTR 22308

To appear in: *Journal of Molecular Structure*

Received Date: 1 December 2015

Revised Date: 28 February 2016

Accepted Date: 29 February 2016

Please cite this article as: R. Agilandeshwari, V. Meenatchi, S. Meenakshisundaram, Synthesis, growth, structure and characterization of chalcone crystal: A novel organic NLO material, *Journal of Molecular Structure* (2016), doi: 10.1016/j.molstruc.2016.02.099.

Graphical abstract

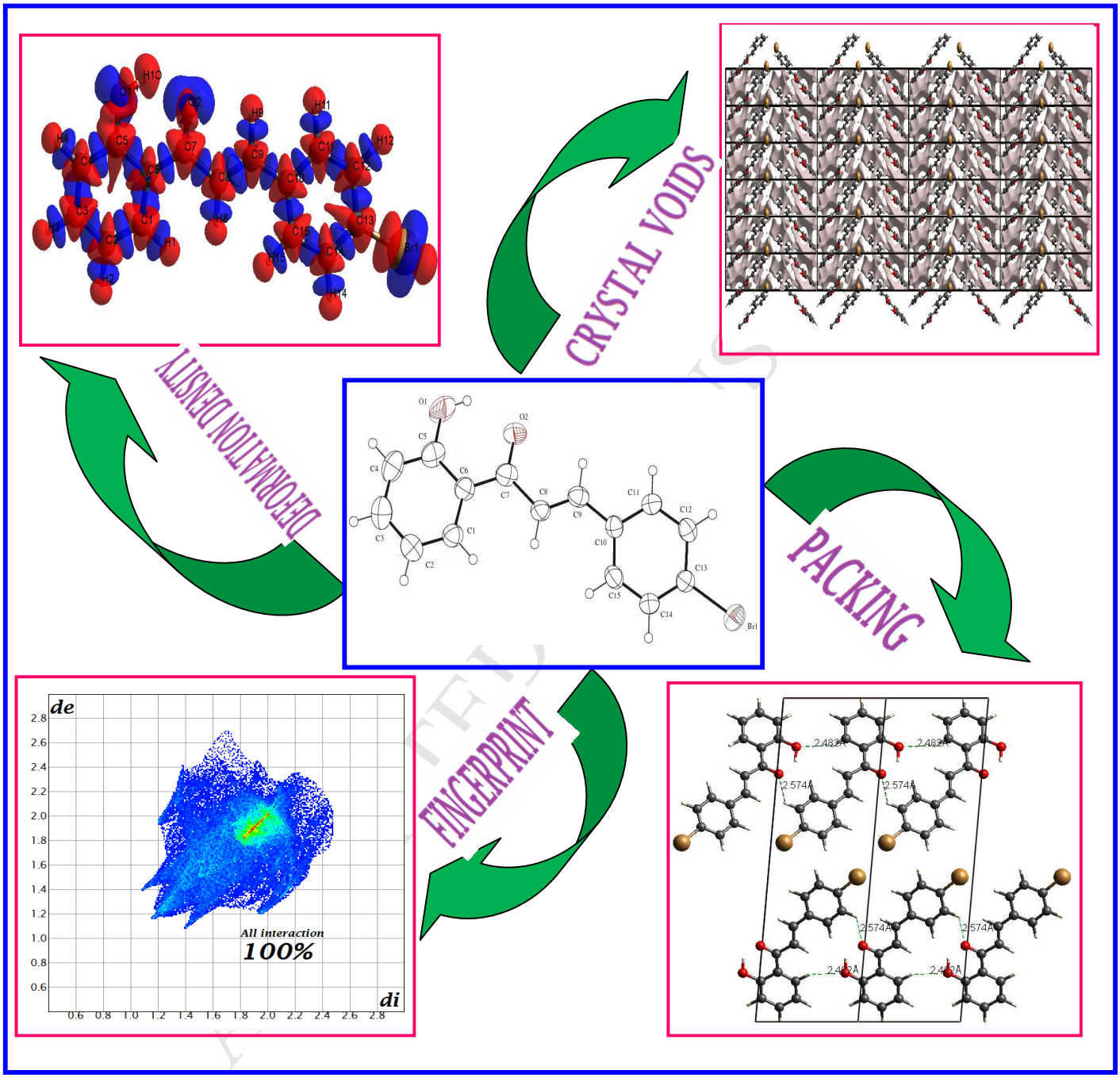

Synthesis, growth, structure and characterization of chalcone crystal: A novel organic NLO material

R. Agilandeshwari[a], V. Meenatchi[a,b] and SP. Meenakshisundaram[a*]

[a]*Department of Chemistry, Annamalai University, Annamalainagar-608 002, Tamil Nadu, India.*

[b]*Department of Chemistry, Sri Vijay Vidyalaya College of Arts and Science (women), Nallampalli, Dharmapuri - 636 807, Tamil Nadu*

Abstract

Single crystals of a chalcone, (E)-3-(4-bromophenyl)-1-(2-hydroxyphenyl)prop-2-en-1-one (BHP), were grown by the slow evaporation solution growth technique. The structure is elucidated by single-crystal X-ray diffraction analysis and the crystal belongs to the monoclinic system with noncentrosymmetric space group $P2_1$. Optical studies reveal that the absorption is minimum in the visible region and the cut-off wavelength is at ~ 468 nm. The band-gap energy was estimated by the application of the Kubelka–Munk algorithm. The powder X-ray diffraction pattern reveals the good crystallinity of the as-grown specimen. The vibrational patterns in FT–IR are used to identify the functional groups and thermal studies indicate the stability of the material. The second harmonic generation efficiency (SHG), as estimated by Kurtz and Perry powder technique, reveals the superior nonlinear optical character of this material. Hirshfeld surface analysis is done to quantify the intermolecular interactions, responsible for developing a nonlinear atmosphere. As-grown crystals were further characterized by SEM, NMR, mass spectrometry and elemental analysis.

* *Corresponding author*
Tel: 0091-4144-221670
Email: aumats2009@gmail.com.

Keywords

X–ray diffraction, Optical properties, Thermal analysis, Hydrogen bonding interactions, SHG efficiency.

1. Introduction

Chalcones and their derivatives possess antioxidant, antibacterial, antifungal, antitumor and anti–inflammatory properties [**1–4].** Organic molecules exhibiting second–order nonlinear optical (NLO) properties have been synthesized and designed for application in optical communications, optical computing, data storage, harmonic generators, frequency mixing and optical switching [**5,6].** Among many organic NLO materials, chalcone derivatives are known for their excellent blue light transmittance [**9–11].** Recently, we have investigated the synthesis, structure, growth and characterization of some chalcones [**12-17].** Mostly they crystallize centrosymmetrically and nonlinearity is not sustained at the macro level due to orientation and packing. Interestingly, the title compound crystallizes in a polar space group. The growth, structure, characterization and NLO response of (E)-3-(4-bromophenyl)-1-(2-hydroxy-phenyl)prop-2-en-1-one (BHP) are reported in the present study.

2. Experiments

2.1. Synthesis

BHP was synthesized by Claisen–Schmidt condensation reaction **[18].** The analytical grade starting materials, *p*-bromo- benzaldehyde (Sigma Aldrich) and *o*-hydroxyacetophenone (Sigma Aldrich) were used as such. 10 % sodium hydroxide solution was taken in a conical flask. A mixture of *p*-bromobenzaldehyde (0.01 mol) and *o*-hydroxyacetophenone (0.01 mol) dissolved in ethanol (50 ml) was added dropwise to the conical flask with vigorous stirring **(Scheme 1).**

During the synthesis, the temperature was maintained between 20–25 °C. After completely adding the aldehyde–ketone mixture, the solution was stirred for another 60 min. Then the reaction mixture was poured in ice cold water and neutralized with dilute hydrochloric acid. The separated product was then filtered and washed with excess of water and finally dried. The synthesized crude sample was purified by successive recrystallizations from ethanol.

2.2. Crystal growth

The crystals were grown by the slow evaporation technique at room temperature. A saturated solution of BHP was obtained by dissolving the sample in ethanol with continuous stirring at room temperature. This solution was filtered using filter paper, slightly warmed and allowed to evaporate very slowly. After about 7 days, good quality, transparent, needle shaped pale yellow crystals started growing. The photographs of the needle shaped as–grown crystal are shown in **Fig. 1**.

3. Results and Discussion

3.1 . FT-IR spectroscopy

FT–IR spectrum of as–grown specimen **(Fig. 2)** was recorded using AVATAR 330 FT–IR by KBr pellet technique in the spectral range of 400–4000 cm^{-1}. The sharp absorption band at ~1658 cm^{-1} is due to carbonyl stretching of α,β–unsaturated carbonyl group. The medium intensity bands around ~2923 and ~2854 cm^{-1} are due to aliphatic C-H stretching vibrations. The sharp absorption band at ~668 cm^{-1} is assigned to C-Br stretching vibration. The strong absorption bands at ~1604 and ~1485 cm^{-1} are corresponding to C=C stretching vibration. The observed FT–IR vibrational bands are listed in **Table S1.**

3.2 . Powder X-ray diffraction analysis

BHP was finely powdered and subjected to powder XRD analysis using a Philips X'pert Pro Triple-axis X–ray diffractometer at room temperature using a wavelength of 1.540 Å and a step size of 0.008°. The samples were examined with Cu K_α radiation in 2θ range of 10–50°. The indexed powder XRD pattern of as–grown specimen is shown in **Fig. S1** along with simulated one. The XRD profiles show that a sample is of single phase without any detectable impurity. The well defined Bragg's peaks at specific 2θ angles show high crystallinity of the material. Most of the peak positions in powder method and simulated XRD pattern derived from single crystal XRD coincide. Differences in mosaic spread of powder and single crystal patterns, and preferred orientations of the sample possibly result in significant intensity variations, as expected.

3.3. Thermal study

In order to test the thermal stability of BHP the thermogravimetric analysis (TG) and differential thermal analysis (DTA) have been carried out simultaneously using NETZSCH STA 449F3 thermal analyzer in nitrogen atmosphere. The TG/DTA thermogram of the BHP is shown in **Fig. S2**. Weight losses due to decomposition are observed at ~230 and 280 °C. An endothermic transition at ~130 °C indicates the melting point of the specimen and it was confirmed by using Sigma instrument (127–131 °C) melting point apparatus. The absence of endo or exothermic transition below 130 °C indicates the crystal stability.

3.4. Scanning electron microscopy (SEM)

The SEM images were taken at maginification values for 250X and 500X with maximum values of 15 kV using a JEOL JSM 5610 LV scanning electron microscope. The SEM images are shown in **Fig. 3.** Bar like shape with surface imperfections are observed.

3.5. Optical studies

Diffuse reflectance spectra of the samples were recorded in the region 200-800 nm using the DRA-CA-30I accessory and converted to absorption spectra using the Kubelka–Munk function. The UV-DRS spectrum was measured in the region of 200–800 nm. The optical reflection spectrum **(Fig. S3 see supplementary data)** shows good reflectance in the visible region and the lower cut–off wavelength is ~468 nm. The Kubelka – Munk theory **[19]** provides a correlation between reflectance and concentration. From the Tauc plots, [*F(R)hv*] as a function of *hv* where *F(R)* is Kubelka – Munk fuction, indirect and direct band gap energies of the specimen are deduced as 2.69 and 2.89 eV respectively, as shown in **Fig. 4.**

3.6. Nuclear magnetic resonance (NMR) spectroscopy

^{1}H NMR and ^{13}C NMR spectra were recorded on BRUKER AVIII 400 MHz NMR spectrometer operating at 400.13 MHz for ^{1}H and 100.61 MHz for ^{13}C using standard parameters. BHP is dissolved in 0.5 ml of $CDCl_3$ solvent and TMS (tetramethylsilane) was used as an internal standard.

The ^{1}H-NMR spectrum of BHP is shown in **Fig. S4a (see supplementary data).** There is a sharp singlet at 12.77 ppm corresponding to OH proton of the phenolic group. The two

doublets at 9.26 and 7.86 ppm are due to α,β-unsaturated proton of the aliphatic group. The aromatic phenyl protons appeared in the range of 6.95-7.67 ppm corresponding to eight protons.

The ^{13}C-NMR spectrum is shown in **Fig. S4b (see supplementary data).** The weak signal at 193.5 ppm corresponds to the carbonyl carbon. The hydroxyl substituted carbon appeared at 163.6 ppm. The signals at 144.0 and 118.9 ppm are due to α,β-unsaturated carbon. The aromatic phenyl carbons appeared in the range of 118.7-136.6 ppm.

3.7. Mass spectrometry

Mass spectra were recorded on a LCMS-2010A Report spectrometer using electron impact technique **(Fig. S5) (see supplementary data).** The molecular ion peak observed at m/z = 303 [$(M)^+$] is in good agreement with the calculated molecular weight. These observations are well supported by single crystal XRD analysis.

3.8. Elemental analysis

Elemental data are collected by FLASH EA 1112 series of CHN analysis. BHP was finely powdered and subjected to elemental analysis. The calculated values of carbon and hydrogen coincide with experimental values **(Fig. S6) (see supplementary data).** Molecular formula = $C_{15}H_{11}BrO_2$; C = 59.43 (cal), 59.62 (exp); H= 3.66 (cal), 3.58 (exp).

3.9. Single crystal X-ray diffraction analysis

The structural analysis of BHP was carried out for a selected sample of approximately 0.25 x 0.16 x 0.10 mm^3 using Bruker AXS (Kappa APEXII) X–ray diffractometer with Mo K_α radiation (λ = 0.71073 Å). The structures were solved and refined by full matrix least squares on F^2 with WinGx software package utilizing SHELXS97 and SHELXL97 modules.

It belongs to the monoclinic system with noncentro- symmetric space group $P2_1$ and the cell parameters are, a = 6.9540 (6) Å, b = 4.0025 (3) Å, c = 22.8414 (18) Å, α = 90°, β = 94.768 (3)°, γ = 90°, V = 633.55 (9) $Å^3$ and Z = 2. The *ORTEP* and packing diagram are shown in **Fig. 5** and the crystal data are listed in **Table 1.** The crystal stability and cohesion are achieved by intermolecular C-H···O hydrogen bonds. Crystal packing diagram along 'a' and 'b' axis are shown as **Figs. 6-7.**

3.10. Hirschfield surface analysis

Hirshfeld surfaces are generated from the crystal data using the DFT method with 6-31G(d) as basis set. The Hirshfeld surfaces of BHP are displayed in **Fig. 8**, showing surfaces that have been mapped over a *dnorm*, *de*, *di*, *shapeindex* and curvedness **[20-22].** The surfaces representing the circular depressions (deep red) visible on the Hirshfeld surface are indicative of hydrogen bonding contact spots due to O-H…O (7.5 %) interactions (**Fig. 8a)** and O…H (7.5 %), H…O (6.5 %), H…H (41.2 %), Br…H (7.6 %) contacts (**Fig. 8c).** The deep red colour spots in *di* **(Fig. 8d)** are strong interactions such as H…Br (4.1%), H…H (41.2 %) and H…O (6.5 %). The *shapeindex* **(Fig. 8b)** surface indicates the electron density surface shape around the molecular interactions. The small range of area and light color on the surface represents a weaker and longer contact other than hydrogen bonds. The *curvedness* surface **(Fig. 8e)** indicates the electron density surface curves around the molecular interactions. The surfaces in the crystal packing along the b-axis **(Fig. 9)** clearly indicate the C-H…O interactions. Graphical images of crystal voids, empty regions present in the crystal lattice packing along a, b and c axes are shown in **Fig. 10.** The deformation density represents difference between the total electron density of a molecule and the electron density of "neutral spherical unperturbed atoms" superimposed at the

same of the molecule. Deformation density clearly explains the surface interaction energy of every atom and bond present in the BHP as shown in **Fig. 11.**

3.11 Fingerprint analysis

Fingerprint plots **[23]** are generated from the crystal data using the DFT method with 6-31G(d) as basis set for evidencing and quantifying the intermolecular interaction patterns. The O…H (7.5 %) interactions are represented by a spike in the bottom area (**Fig. 12**) whereas the H…O (6.5 %) interactions by a spike in the top left region. Hydrogen-hydrogen interactions, H…H (41.2 %) are very high compared to the other bonding interactions. Sharp curved spike at the bottom right area indicates the Br…H (7.6 %) and top left corner with curved spike indicates the H…Br (4.1 %). The finger print at the bottom right area represents C…H (6.0 %) interactions and top right area represents H…C (4.0 %) interactions. The finger print at the top centre area represents C…Br (1.1 %), Br…C (1.2 %), C…C (15.8 %), O…O (0.8 %), C…O (0.4 %), O…C (0.4 %) and Br…Br (3.2 %) interactions. Strong interactions occupy more space and weak interactions occupy less space in the fingerprint plot. The combination of *de* and *di* in the form of a two-dimensional fingerprint plot provides a summary of intermolecular contacts in the crystal. Relative contributions of various intermolecular interactions in BHP are shown in **Fig. 13.**

3.12 Second harmonic generation efficiency

In order to confirm the influence of the nonlinear optical properties of the as-grown specimen, it was subjected to SHG test using Kurtz and Perry **[24]** technique. The output gives relative nonlinear optical efficiencies of the measured specimens. The doubling of frequency was confirmed by the green color of the output radiation of characteristic wavelength 532 nm. With an input beam energy of 5.70 mJ/pulse, KDP sample was used as reference

material ($I_{2\omega}$ =102 mV) and the powder SHG efficiency of BHP was found to be superior to that of KDP ($I_{2\omega}$= 536 mV).

Large first-order hyperpolaraizability *(β)* of magnitude about ~85 times that of urea, as estimated by density functional theory (DFT) method with 6-31G(d,p) as the basis set and a significant SHG- activity nearly five times that of KDP clearly substantiate the NLO response of the chalcone. Higher the *β*, highest the charge transfer.

Organic molecules containing extended π-conjugation are characterized by large values of the second harmonic generation efficiency showing significant NLO activity. The strong inter- and intramolecular hydrogen bonding enhances charge transfer and it is responsible for nonlinear optical character.

4. Conclusion

Transparent needle like crystals of *(E)*-3-(4-bromophenyl)-1-(2-hydroxyphenyl)prop-2-en-1-one were grown in ethanol by the slow evaporation solution growth technique at room temperature. The product formation was confirmed by FT–IR, NMR, LC–Mass, elemental analysis and single crystal XRD analysis. The crystallographic data indicate that the specimen crystallizes in the monoclinic system with noncentrosymmetric space group $P2_1$. TG/DTA study reveals the purity of the sample and no decomposition is observed up to the melting point. The analysis of the Hirshfeld surface derived fingerprint plots is shown to be an effective method to identify and quantify various types of intermolecular interactions. A superior SHG-activity clubbed with high *β* caused by inter- / intramolecular interactions and close packing prove this chalcone as a promising NLO candidate.

Supporting Information

CCDC 1043959 contains the supplementary crystallographic data for this paper. These data can be obtained free of charge from The Cambridge Crystallographic Data Centre via www.ccdc.cam.ac.uk/data request/cif. Supplementary information contains Powder X-ray diffraction, thermal study, UV-DRS, NMR, LC-mass, elemental analysis and FT-IR table.

Acknowledgements

The authors thank the UGC-Networking Resource Centre, School of Chemistry, University of Hyderabad, for providing characterization facility. One of the authors Dr. V. Meenatchi expresses her sincere gratitude to Dr. R. Chandrasekar, Associate Professor, for providing lab facilities in University of Hyderabad. The authors thank the Council of Scientific and Industrial Research (CSIR), New Delhi, for financial support through research grant No.03(1233)/12/EMR-II and Dr. V. Meenatchi is grateful to CSIR project for the award of Research Associate (RA).

References

[1] S.F. Nielsen, S.B. Christensen, G. Cruziani, A. Kharazmi, T. Liljefors, J. Med. Chem. 41 (1998), 4819-4832.

[2] M. Liu, P. Wilairat, M.L. Go, J. Med. Chem. 44 (2001) 4443-4452.

[3] J. Rojas, J.N. Dominguez, J.E. Charris, G. Lobo, M. Paya, M.L. Ferrandiz, Eur. J. Med. Chem.37(2002) 699-755.

[4] V. Calvino, M. Picallo, A.J. Lopez-Peinado, R.M. Martın-Aranda, C.J. Duran-Valle, Appl. Surf. Sci. 252 (2006) 6071-6074.

[5] D.S. Chemla, J. Zyss. Academic. Press. 1987, New York.

[6] P.N. Prasad and D.J. Williams, Wiley. 1991, New York.

[7] J.L. Oudar, D.S. Chemla, J. Chem. Phys. 66 (1977) 2664-2668.

[8] J.L. Oudar, J. Chem. Phys. 67 (1977) 446-457.

[9] B. Zhao, W.Q. Lu, Z.H. Zhou, Y. Wu, J. Mater. Chem. 10 (2000) 1513-1515.

[10] D. Fichou, T. Watanabe, T. Takeda, S. Miyata, Y. Goto, M. Nakayama, Jpn. J. Appl. Phys. 27 (1988) L429-L434.

[11] Y. Goto, A. Hayashi, Y. Kimura, M. Nakayama, J. Cryst.Growth 108 (1991) 688-698.

[12] K. Vanchinathan, G. Bhagavannarayana, K. Muthu, S.P. Meenakshisundaram, Physica B 406 (2011) 4195-4199.

[13] M. Rajasekar, K. Muthu, G. Bhagavannarayana, S.P. Meenakshisundaram, J. Appl. Cryst. 45 (2012) 914-920.

[14] V. Meenatchi, K. Muthu, M. Rajasekar, SP. Meenakshisundaram, Physica B 419 (2013) 95–99.

[15] V. Meenatchi, K. Muthu, M. Rajasekar, S.P. Meenakshisundaram, Spectrochim. Acta A. 120 (2014) 72-76.

[16] S. Sudha, N. Sundraganesan, K. Vanchinathan, K. Muthu, S.P. Meenakshisundaram, J. Mol. Struct. 1030 (2012) 191-203.

[17] V. Meenatchi, K. Muthu, M. Rajasekar, SP. Meenakshisundaram, Mol. Cryst. Liq. Cryst. 609 (2015) 171–182.

[18] A.I. Vogel, Practical Organic Chemistry., 5th ed, 1989.

[19] P. Kubelka, F. Munk, Z. Tech. Phys. 12 (1931) 593-595.

[20] M.A. Spackman, D. Jayatilaka, Cryst.Eng.Comm. 11 (2009) 19-32.

[21] F. L. Hirshfeld, Theor. Chim. Acta.44 (1977) 129–138.

[22] CrystalExplorer (Version 3.1), S.K. Wolff, D.J. Grimwood, J.J. McKinnon, M.J. Turner, D. Jayatilaka, M.A. Spackman, University of Western Australia, 2012.

[23] M.A. Spackman, J.J. McKinnon, Cryst.Eng.Comm. 4 (2002) 378-392.

[24] S. K. Kurtz, T. T. Perry, J. Appl. Phys. 39 (1968) 3798-3813.

Table 1. Crystal data and structure refinement for BHP

Empirical formula	$\mathbf{C_{15}H_{11}BrO_2}$
Formula weight	303.15
Temperature	296(2) K
Wavelength	0.71073 Å
Crystal system, space group	Monoclinic, $P2_1$
Unit cell dimensions	a = 6.9540(6) Å, α= 90° b = 4.0025(3) Å, β = 94.768(3)° c = 22.8414(18) Å, γ = 90°
Volume	633.55(9) $Å^3$
Z, calculated density	2, 1.589 Mg/m^3
Absorption coefficient	3.234 mm^{-1}
F(000)	304
Crystal size	0.250 x 0.160 x 0.100 mm^3
Theta range for data collection	0.895 to 22.602 °.
Limiting indices	$-6 \le h \le 7, -4 \le k \le 3, -23 \le l \le 24$
Reflections collected/unique	3211 / 1633 [R(int) = 0.0249]
Completeness to theta = 22.20	99.7 %
Absorption correction	None
Refinement method	Full-matrix least-squares on F^2
Data/restraints/parameters	1633 / 2 / 168
Goodness-of-fit on F^2	1.046
Final R indices [I > 2sigma(I)]	R1 = 0.0394, wR2 = 0.0953
R indices (all data)	R1 = 0.0464, wR2 = 0.0992
Absolute structure parameter	0.016(11)
Extinction coefficient	0.002(4)
Largest diff. peak and hole	0.678 and -0.566 e. $Å^{-3}$

Figure captions

Fig 1. Photographs of BHP.

Fig 2. FT–IR spectrum of BHP.

Fig 3. SEM images of BHP.

Fig 4. Tauc plot of BHP (a) direct and (b) indirect band gap energy.

Fig 5. (a) ORTEP (b) packing diagram of BHP.

Fig 6. Crystal packing diagram of BHP along 'a' axis.

Fig 7. Crystal packing diagram of BHP along 'b' axis.

Fig 8. Hirshfeld surfaces of BHP (a) *dnorm* (b) *Shapeindex* (c) *de* (d) *di* (e) *curvedness*.

Fig. 9. Hirshfeld surfaces: (a) *dnorm* in crystal packing with H-bond contacts, (b) *Shapeindex* in crystal packing, (c) *Curvedness* in crystal packing, (d) *de* surface in crystal packing, and (e) *di* surface in crystal packing.

Fig 10. (a) Crystal voids in packing along the a axis (b) Crystal voids in packing along the b axis (c) Crystal voids in packing along the c axis.

Fig 11. (a) Deformation density and (b) hydrogen bonding interactions along with deformation density of BHP.

Fig 12. Fingerprint plots representing quantity of molecular interactions of BHP.

Fig 13. Quantities of molecular interactions represented in a pie chart.

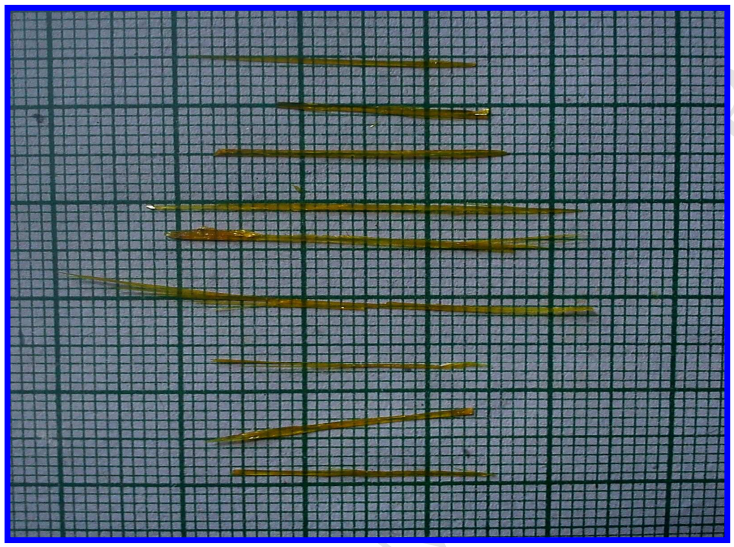

Fig. 1

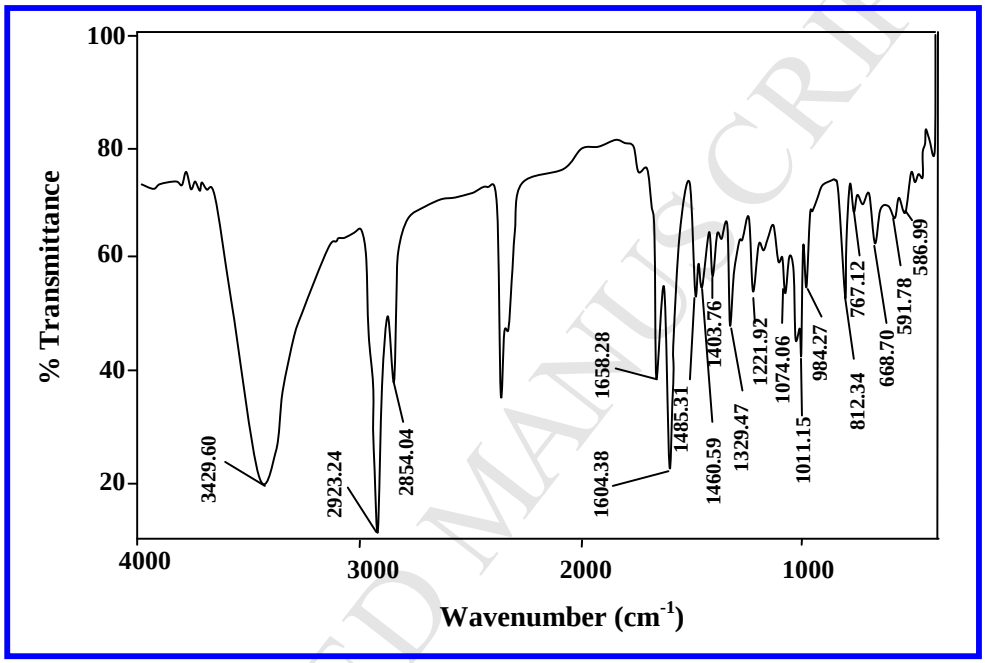

Fig. 2

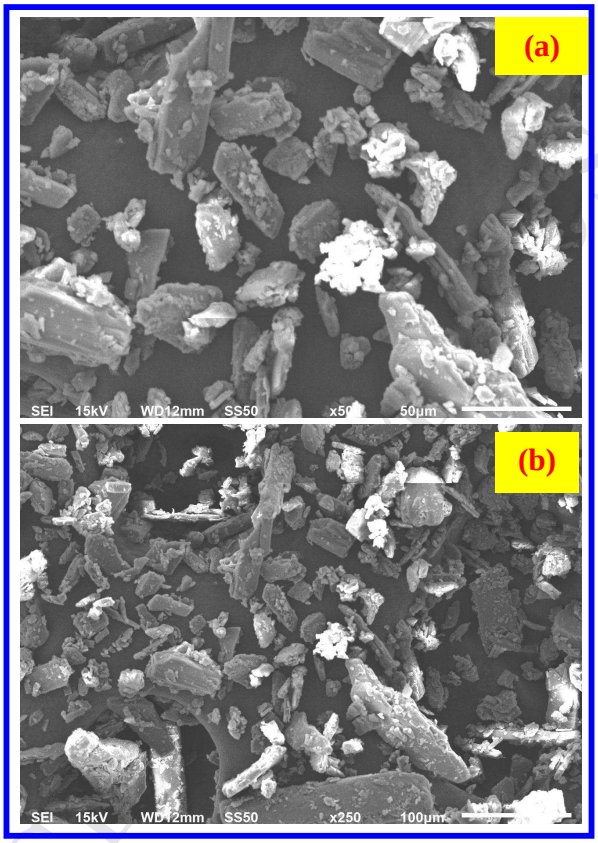

Fig. 3

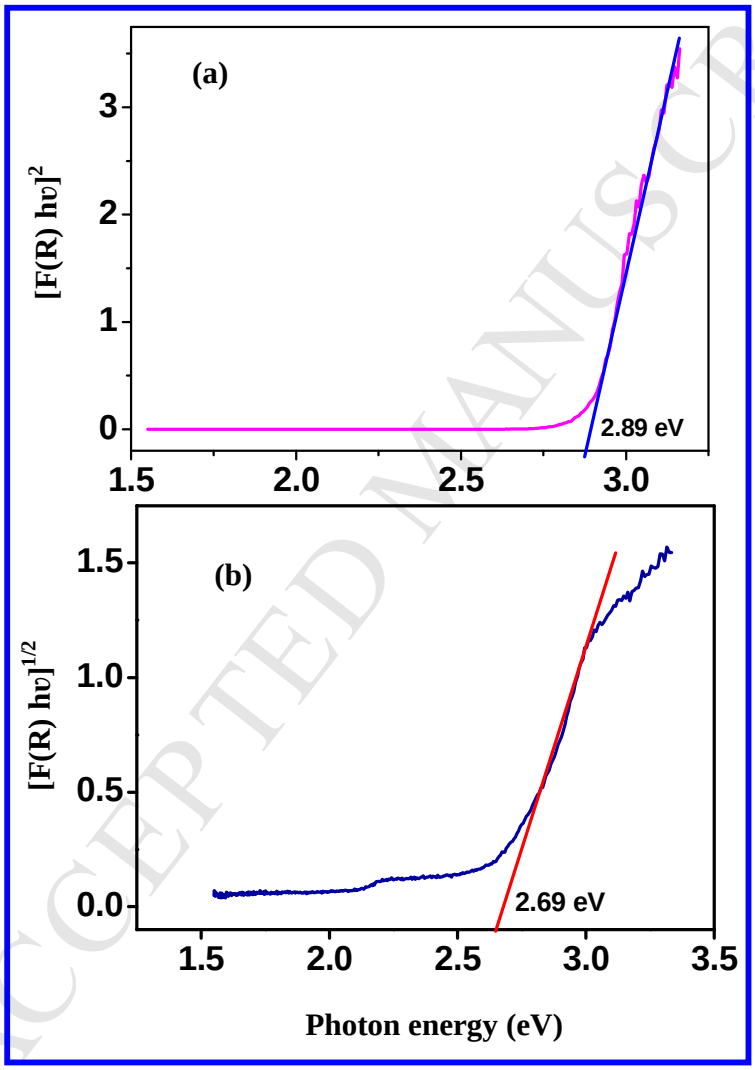

Fig. 4

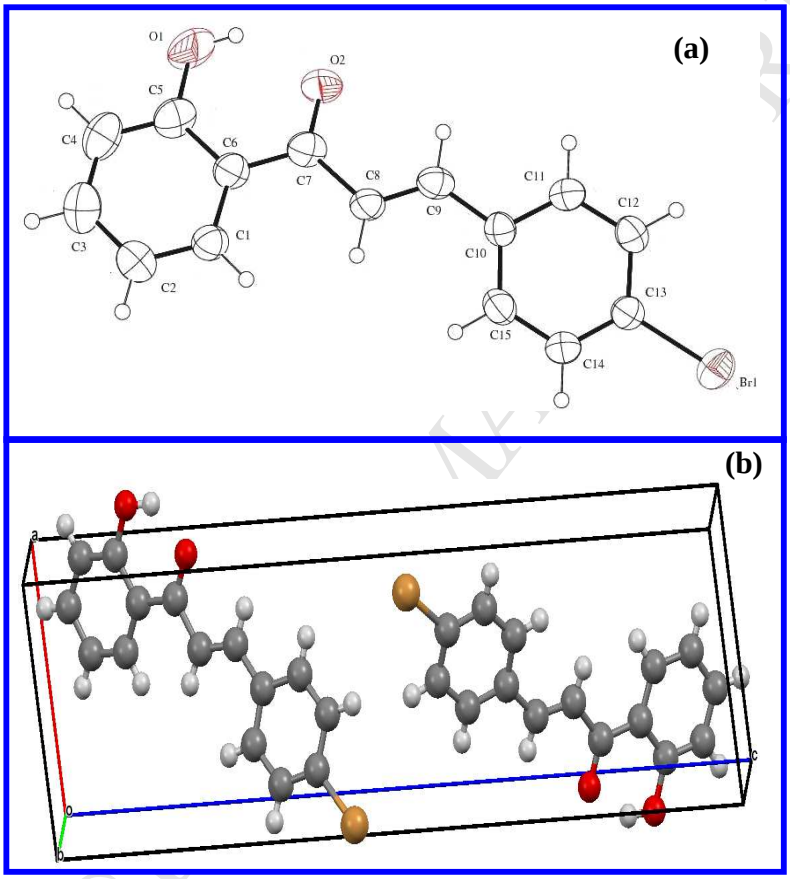

Fig. 5

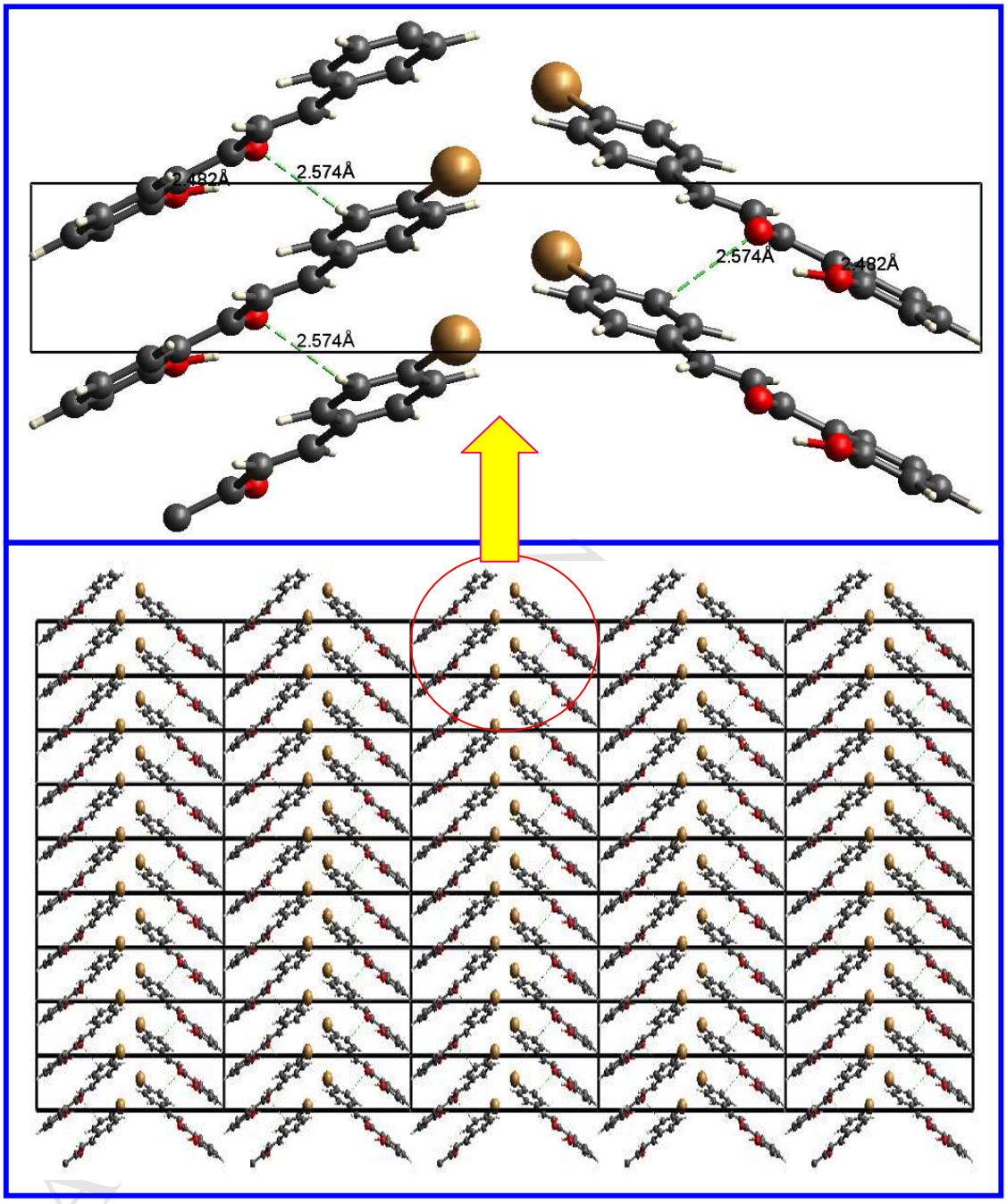

Fig. 6

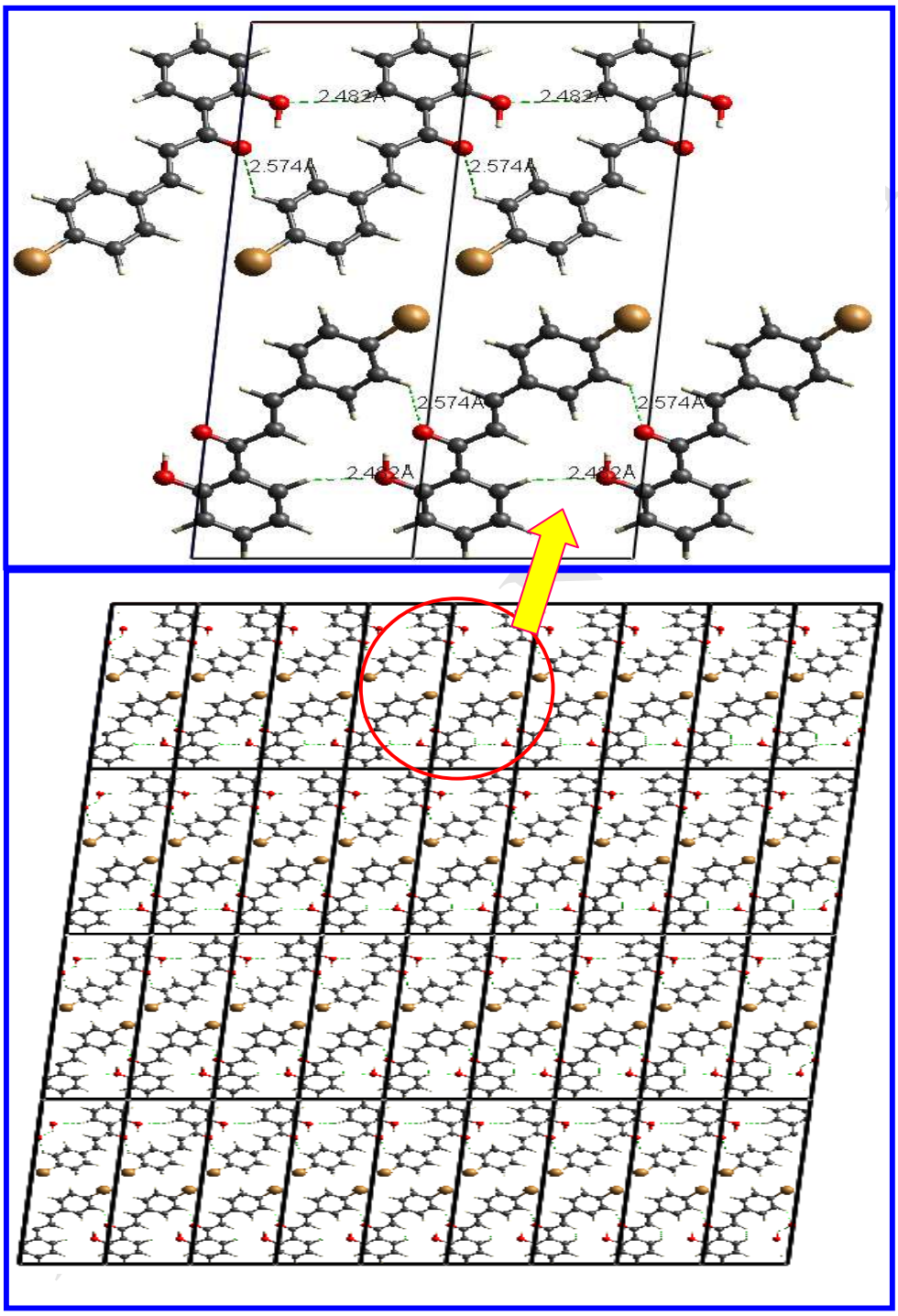

Fig. 7

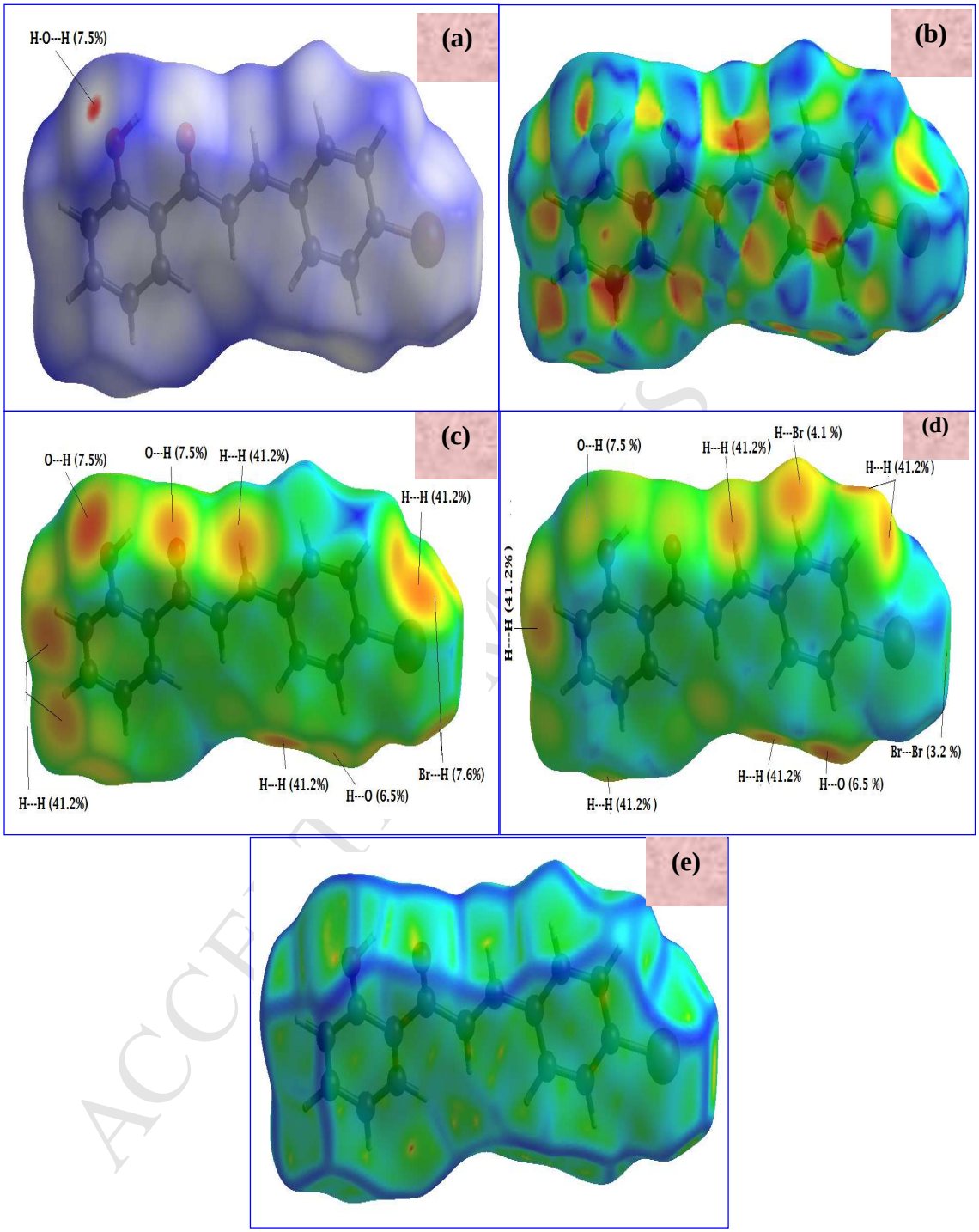
(a)
H-O···H (7.5%)
(b)
(c)
O···H (7.5%)
O···H (7.5%)
H···H (41.2%)
H···H (41.2%)
H···H (41.2%)
Br···H (7.6%)
H···H (41.2%)
H···O (6.5%)
(d)
O···H (7.5 %)
H···H (41.2%)
H···Br (4.1 %)
H···H (41.2%)
H···H (41.2%)
Br···Br (3.2 %)
H···H (41.2%)
H···O (6.5 %)
H···H (41.2%)
(e)

Fig. 8

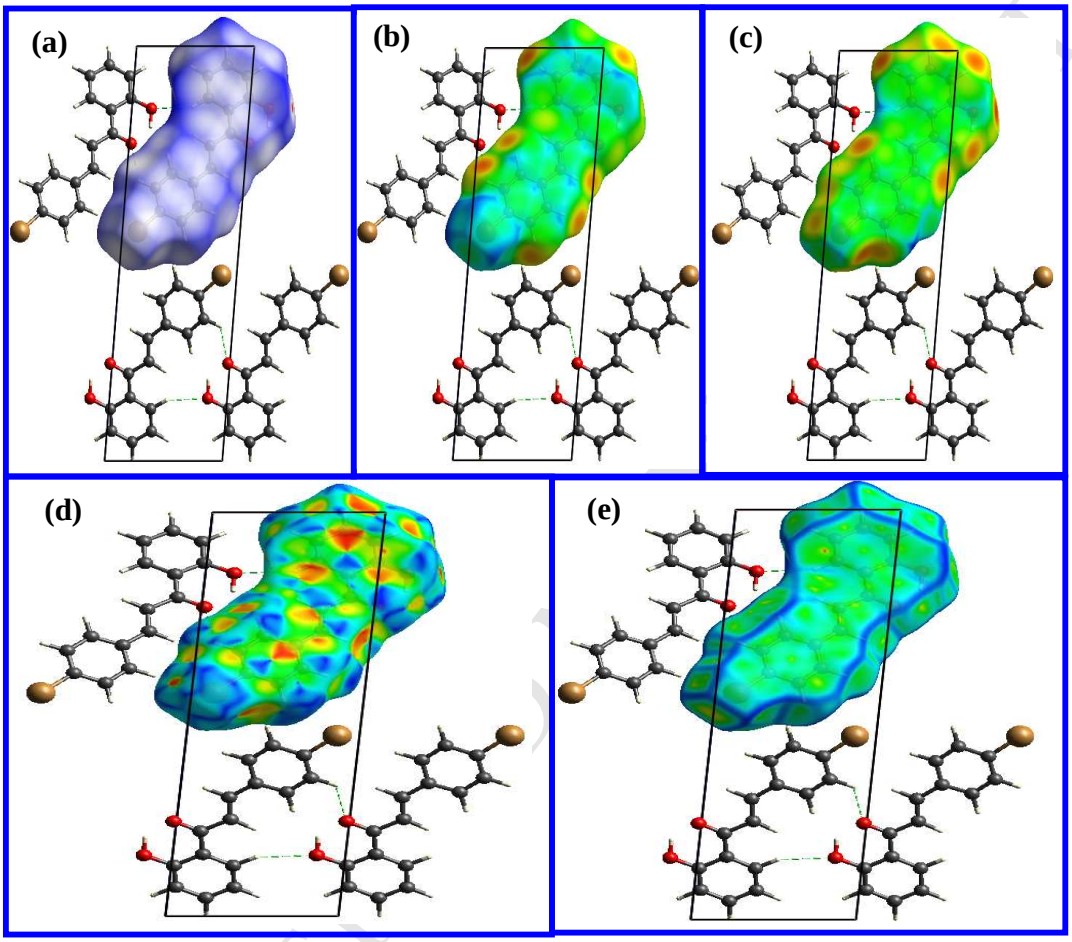

Fig. 9

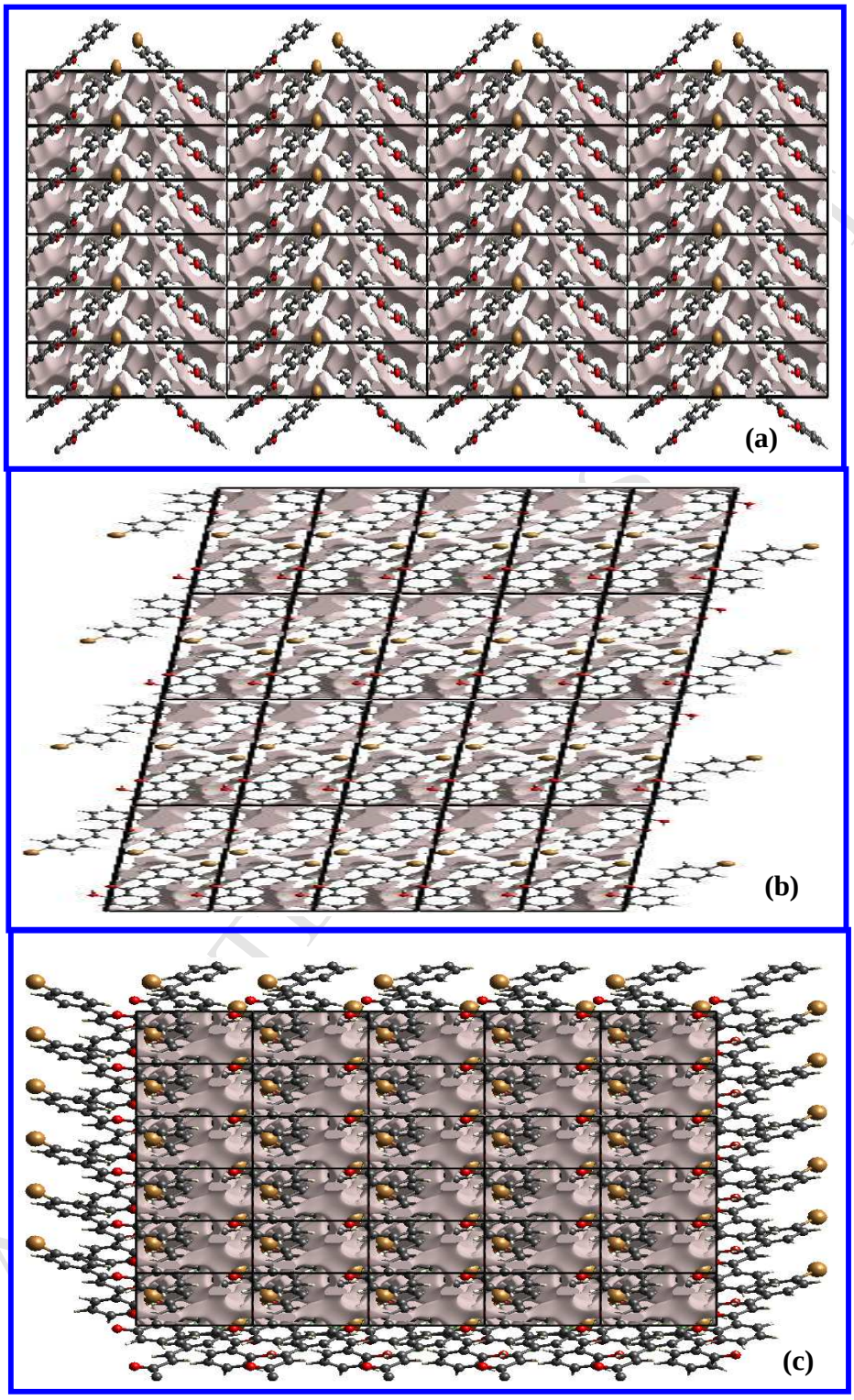

Fig. 10

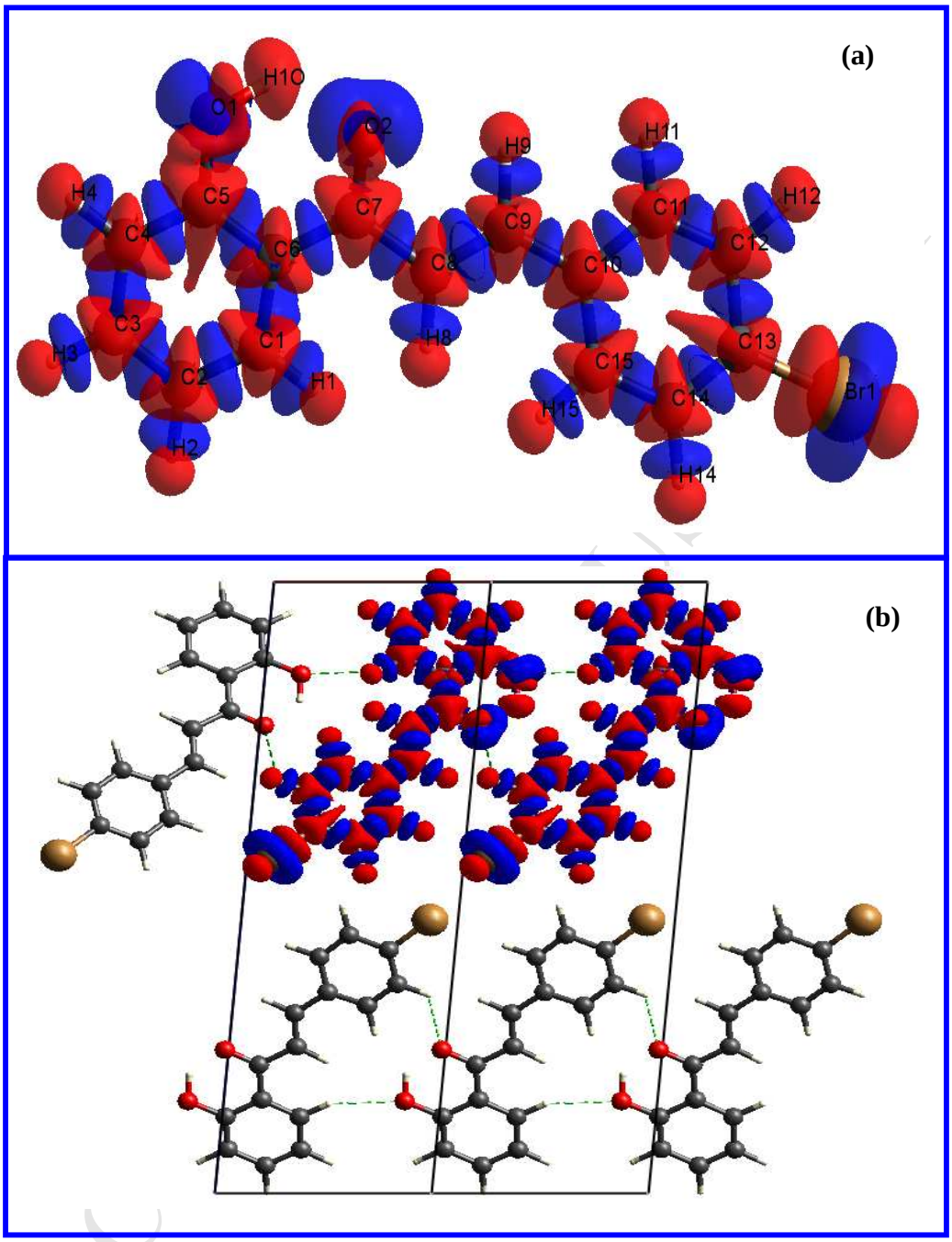
(a)
H10
O1
O2
H9
H11
H4
C5
C7
C9
C11
H12
C4
C6
C8
C10
C12
C3
C1
H8
C13
H3
C2
H1
C15
Br1
C14
H15
H2
H14
(b)

Fig. 11

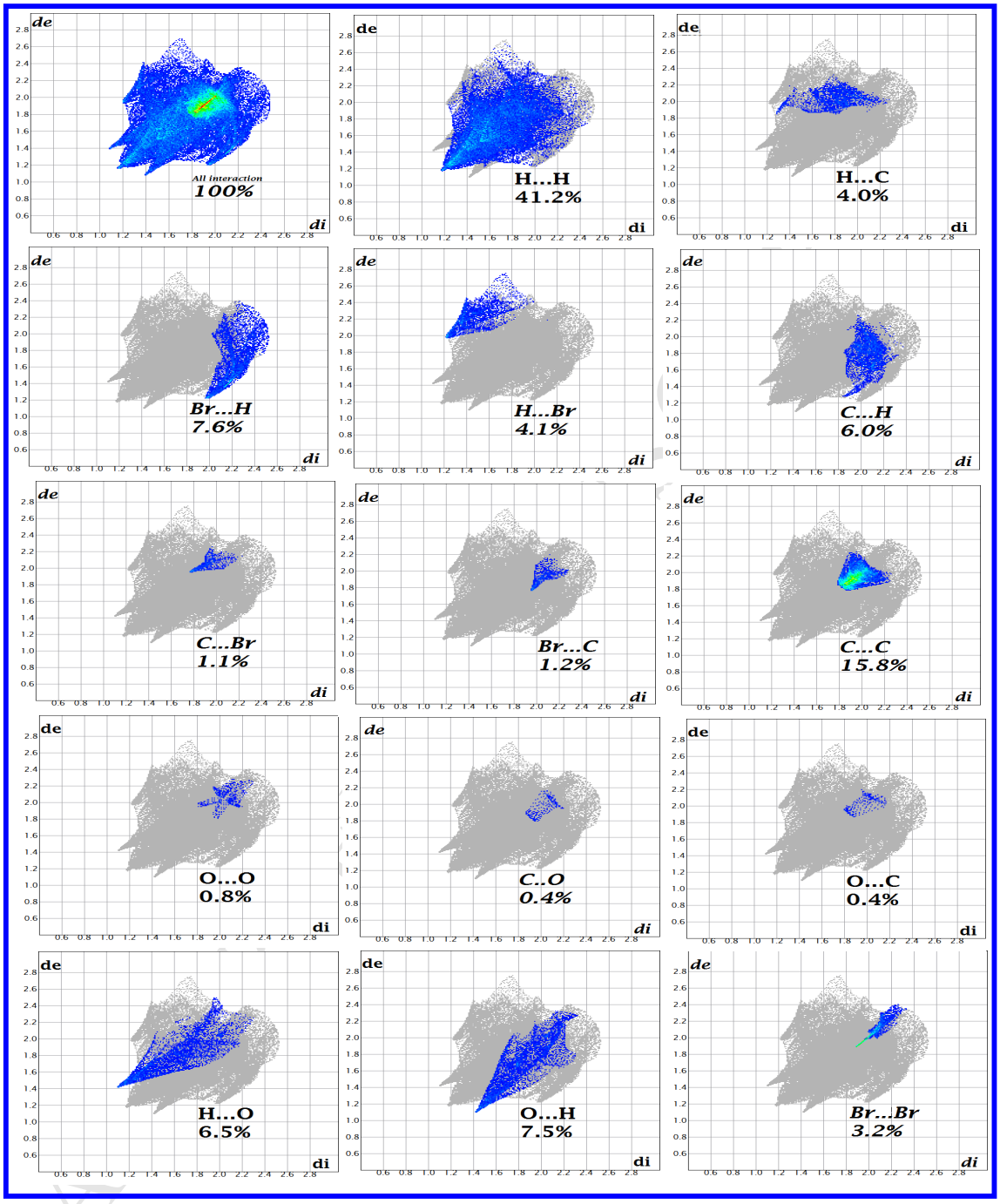
de
di
All interaction
100%
H...H
41.2%
H...C
4.0%
Br...H
7.6%
H...Br
4.1%
C...H
6.0%
C...Br
1.1%
Br...C
1.2%
C...C
15.8%
O...O
0.8%
C..O
0.4%
O...C
0.4%
H...O
6.5%
O...H
7.5%
Br...Br
3.2%

Fig. 12

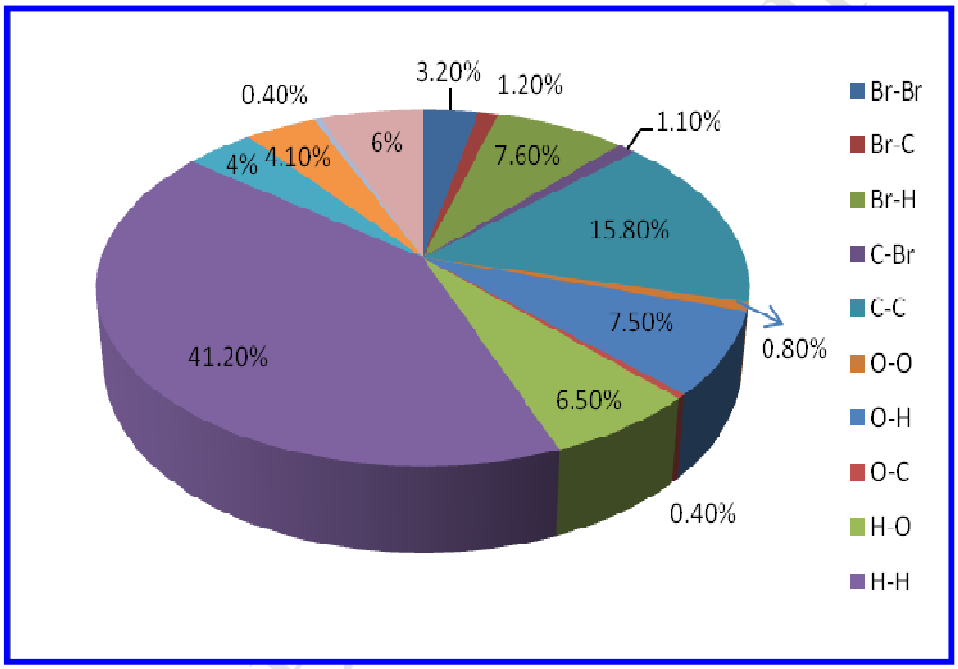

Fig. 13

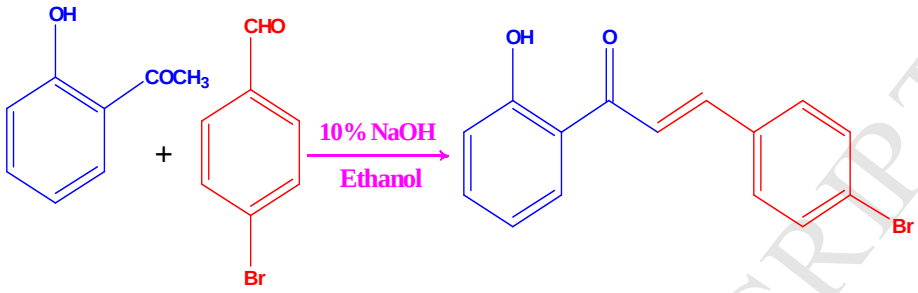

Scheme 1

Research Highlights

- Growth of a new organic NLO active crystal, a chalcone derivative is reported.
- Band gap energy is estimated by Kubelka- Munk function.
- Structure is elucidated and inter-/intramolecular hydrogen bonding interactions are analyzed by Hirshfeld surface and fingerprint analysis.
- Superior NLO activity than the reference material KDP is observed.